On the modelling of experimental results on plasma shaping with a synthetic diagnostic and nonlinear gyrokinetic GENE simulations

A. Iantchenko[1], G. Merlo[2], F. Carpanese[1], M. Vallar[1], S. Brunner[1], S. Coda[1]

[1] *Ecole Polytechnique Fédérale de Lausanne (EPFL), Swiss Plasma Center (SPC), CH-1015 Lausanne, Switzerland*

[2] *University of Texas at Austin, Austin, United States*

We report on modelling of localised measurements of turbulent electron density fluctuations obtained with the Tangential Phase Contrast Imaging diagnostic (TPCI) installed on the TCV tokamak [1, 2]. Nonlinear flux-tube gyrokinetic (GK) simulations are performed with the Eulerian (grid-based) GENE code [3], taking into account realistic TCV geometry and profiles. A synthetic diagnostic [4] has been developed in MATLAB and is applied to the simulated density fluctuations to model the experimental measurement procedure, allowing detailed comparison between simulation and experiment.

We consider the positive triangularity ($\delta = 0.5$) and negative triangularity ($\delta = -0.25$) TCV discharges, #49052 and #49051 respectively, both with equal amount 460kW of ECH heating. To address the issue of the high sensitivity of GK results to variation of input parameters within experimental uncertainties, we attempt to use a Kinetic Equilibrium Reconstruction (KER) [5] and a Quasi-Linear (QL) [6] analysis. The aim of KER is to identify the plasma state given available measurements of profiles and/or first principle modelling. This is achieved by iterating over pressure profiles combined with a calculation of the deposited heat and current drive, and a reconstruction of the plasma equilibrium. The computation is run until convergence when all results match available constraints in a least-square sense. As input to KER we provide the electron pressure measured by the Thomson diagnostic, while the ion density is estimated from quasi-neutrality and the ion temperature is taken to be proportional to the electron temperature.

The next step is to further tune the results from KER by computing QL predictions of non-linear heat and particle fluxes from computationally inexpensive linear GK simulations obtained with GENE. Most important input parameters can then be varied until the QL predictions satisfy the experimental constraints. For the considered discharges, two experimental constraints on QL results are known. These are the electron-to-ion heat flux ratio Q_e/Q_i and the particle flux-to-heat flux ratio Γ_s/Q_i. The latter should be vanishing in the case of no external particle injection as is the case in the considered TCV discharges. With the nominal KER input parameters we find the QL predictions $Q_e/Q_i = 1.4$ for $\delta > 0$ and $Q_e/Q_i = 18$ for $\delta < 0$, and a non-vanishing particle flux $\Gamma \neq 0$. The corresponding experimental results are $Q_e/Q_i = 22 \pm 4 (\delta > 0)$ and $Q_e/Q_i = 53 \pm 12 (\delta < 0)$. An attempt was made to vary the input parameters of both scenarios to match the experimental constraints, but the very large uncertainty in the ion pressure profiles (due to the absence of a direct measurement) implies too many degrees of freedom and an

almost arbitrary result from the QL analysis. The QL method was therefore not further pursued in the analysis of the considered scenarios, so that GK simulations were carried out using input parameters generated by KER only.

Non-linear ion scale GENE simulations were carried out to generate electron density fluctuations $\delta n_e(k_x, k_y, z, t)$ for both $\delta > 0$ and $\delta < 0$ scenarios. For both cases we consider local simulations at the radial position $\rho_t = 0.6$, where ρ_t is the square root of the normalised toroidal flux, since TPCI measurements are dominated by contributions at this radius. We consider the grid $N_x \times N_y \times N_z \times N_{v_{||}} \times N_\mu \times N_s = 256 \times 64 \times 48 \times 30 \times 16 \times 3$, where the resolutions refer to the number of discretization points along the three spatial directions (x, y, z), the two velocity space directions $(v_{||}, \mu)$, and the number of particle species s respectively. Impurities (Carbon), collisionality, electromagnetic effects and experimental magnetic geometry were all retained.

For $\delta > 0$, KER provides the normalised species density and temperature gradients $a/L_{n,e} = 1.48, a/L_{T,e} = 2.8, a/L_{T,i} = 3.75$ (a is the plasma minor radius), electron-ion temperature ratio $T_i/T_e = 0.26$, electron-carbon density ratio $n_c/n_e = 0.05$, safety factor $q_0 = 1.46$, and magnetic shear $\hat{s} = 1.25$. For $\delta < 0$ we instead use $a/L_{n,e} = 1.13, a/L_{T,e} = 3.6, a/L_{T,i} = 3.4, T_i/T_e = 0.22, n_C/n_e = 0.1, q_0 = 1.21$ and $\hat{s} = 1.02$. The radial and binormal simulation box sizes are different for the two scenarios, with $L_x = 128\rho_i, L_y = 112\rho_i$ for $\delta > 0$ (ρ_i is the ion Larmor radius), and $L_x = 142\rho_i, L_y = 152\rho_i$ for $\delta > 0$ as a consequence of the different values of $\hat{s}$ and q_0. For the same number of radial and binormal wave numbers we therefore have $\max(k_y\rho_i) = 3.5, \max(k_x\rho_i) = 6.24$ for $\delta > 0$ and $\max(k_y\rho_i) = 2.6, \max(k_x\rho_i) = 5.6$ for $\delta < 0$.

For the considered parameters, we find the simulated ion and electron heat flux $Q_e = 152\text{kW}, Q_i = 10\text{kW}$ for $\delta > 0$ and $Q_e = 504\text{kW}, Q_i = 3\text{kW}$ for $\delta < 0$. The experimental values are instead $Q_e = 658 \pm 70\text{kW}, Q_i = 10 \pm 5\text{kW}$ for $\delta > 0$ and $Q_e = 616 \pm 70\text{kW}, Q_i = 11 \pm 5\text{kW}$ for $\delta < 0$. In both cases, but especially for $\delta > 0$, we see that GK simulations with KER underestimates the heat flux values. The reduction of the simulated ion heat flux going from $\delta > 0$ to $\delta < 0$ is due to a stabilisation of Ion Temperature Gradient (ITG) modes at the considered scales, which is a combined effect of an increased impurity content, and the change in the plasma shape. While at $\delta < 0$ Trapped Electron Modes (TEM) are also stabilised, this effect is overcome by the destabilisation due to an increased electron temperature gradient, leading to an overall increase in the electron heat flux.

From the non-linear GENE simulations, we obtain the electron density fluctuations $\delta n_e(k_x, k_y, z, t)$ for both $\delta > 0$ and $\delta < 0$ scenarios that are post-processed by a synthetic diagnostic to model measurements from TPCI. The synthetic TPCI signal in the form of a phase shift $\delta\varphi(r, t)$ of the laser light for each detector element distributed along r is computed by integrating δn_e, over the laser beam path L in the plasma

$$\delta\varphi(r,t) = \sum_{k_x,k_y} \int_L \mathrm{d}\ell F(k_x, k_y, z(r,\ell))\delta n_e(t, k_x, k_y, z(r,\ell)) e^{ik_x x(r,\ell) + ik_y y(r,\ell)}, \tag{1}$$

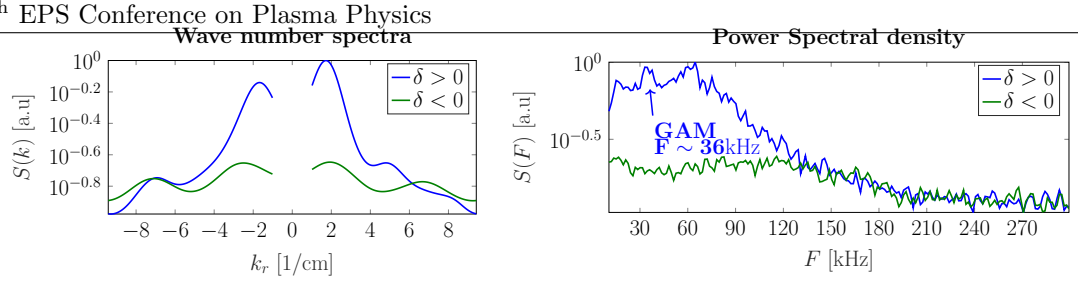

Figure 1: *Experimental wave-number spectra (left), frequency spectra (right); $\delta > 0$ (blue) and $\delta < 0$ (green).*

where ℓ denotes the coordinate along the laser beam. The filter function $F(k_x, k_y, z(r, \ell))$ is used to restrict the directions of the wave vector that contributes in Eq. (1) which translates to a reduction in the integration length L. Best radial localisation $\delta\rho_t$ is obtained for purely radial ($k_y = 0$) modes with $\Delta\rho_t \lesssim 0.05$ centred around the $\rho_t = 0.6$ flux surface that was chosen as the centre of the flux tube in the local GENE simulations. Modes with $k_y \neq 0$ are however less well localised with $\Delta\rho_t \lesssim 0.2$.

At the time of the measurement, the TPCI diagnostic at TCV was equipped with only 9 unevenly spaced functional detector elements (we therefore have $r = r_1 \ldots r_9$ distinct coordinates in Eq. (1)). The maximum measured wave number is $\max(k_r) \approx 9\text{cm}^{-1}$ while $\min(k_r) \approx 1\text{cm}^{-1}$ due to the phase contrast transfer function. The orientation of the filter with respect to the laser beam is chosen such that the filter function $F(k_x, k_y, z(r, \ell))$ favours purely radial ($k_y = 0$) modes. The detector image is aligned with the direction of the filter axis and therefore $k_r \sim k_x$.

The experimental wave-number spectra and frequency spectra are shown in Fig. 1. For $\delta > 0$, it shows that fluctuations propagate dominantly in the positive ($k_r > 0$) direction, with a peak at $k_r \sim 2\text{cm}^{-1}$. The frequency spectra contains a mode at $F \sim 36$kHz, which is typical for a Geodesic Acoustic Mode (GAM) in TCV [7]. A steep power cascade is visible between 80-200kHz and a less steep cascade is seen for 200-300kHz. At $\delta < 0$, the amplitude of the fluctuations with $F < 120$kHz components including the GAM, has been reduced, and $S(k_r)$ now shows no preferential propagation direction. A further interpretation of the experimental result can be done by comparison with the corresponding synthetic result shown in Fig. 2. As in experiments, $S(k_r)$ for $\delta > 0$ is dominant at $k_r \sim 2\text{cm}^{-1}$, which is shown to result from the purely radial $k_y = 0$ fluctuation contributions. These also lead to a peak in frequency at $F \sim 40$kHz, while contributions from $k_y \neq 0$ fluctuations are instead responsible for a power cascade in frequency. An analysis of the raw GENE output has revealed that the $k_y = 0$ density fluctuation component has the poloidal $m = 1$ structure of a GAM. The sign of k_r for the maximum of $S(k_r)$ can be explained by considered measurement geometry of TPCI picking up mainly contributions from the upper midplane of the plasma, where $k_r > 0$ is preferentially selected. At $\delta < 0$, the GAM component is significantly reduced and the signal is instead dominated by $k_y \neq 0$ components that lead to a flat $S(k_r)$ spectrum. In contrast to the experiment, the amplitude

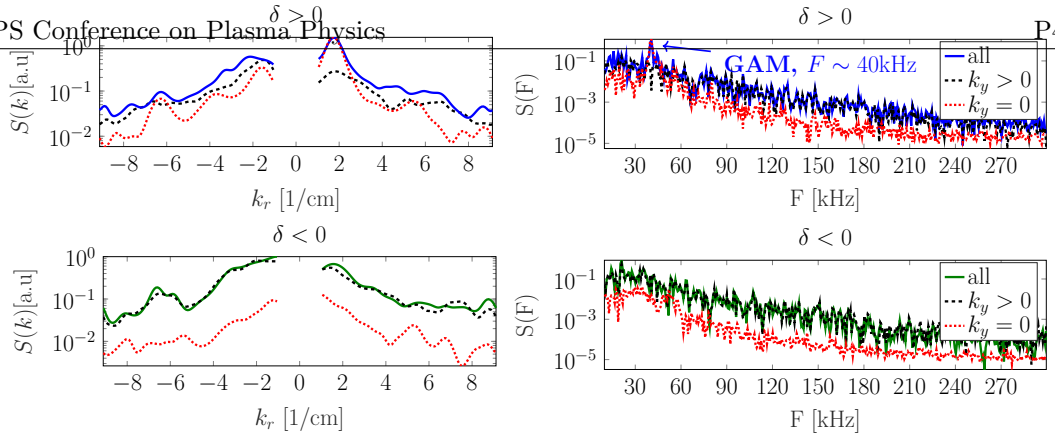

Figure 2: *Synthetic wave-number spectra (left), frequency spectra (right) for $\delta > 0$ (top) and $\delta < 0$ (bottom) cases. The result is shown when including all k_y contributions in Eq.* (1) *(solid blue for $\delta > 0$ and green for $\delta < 0$), only $k_y \neq 0$ (dashed green) and only $k_y = 0$ (dotted red).*

of the fluctuations seems to increase, which is due to the increased TEM contribution seen in the GK simulations. While the features of $k_y = 0$ modes are in good qualitative agreement with experiments, we notice that the frequency cascade in power is very different between experiments and simulations, which suggests that the features of $k_y \neq 0$ modes are not yet correctly captured by the synthetic diagnostic. As mentioned earlier, one potential reason is the reduced localisation of $k_y \neq 0$ mode contributions in Eq. (1), which therefore should be modelled either by multiple flux tubes at different radial locations, or by a single global simulation. Further improvement in the modelling requires also improved GK results, with a larger and equal range of k_y and k_x modes for consistent comparison between $\delta > 0$ and $\delta < 0$, but most importantly better diagnosed discharges, as well as using both KER and the QL method to optimise the input parameters to GENE. Better cases will be investigated in future work, also using an upgraded version of TPCI with more detector elements and potentially ETG scale measurements.

The numerical simulations have been carried out on the EUROfusion High Performance Computer (Marconi-Fusion). This work has been carried out within the framework of the EUROfusion Consortium and has received funding from the Euratom research and training programme 2014-2018 and 2019-2020 under grant agreement No 633053. The views and opinions expressed herein do not necessarily reflect those of the European Commission. This work was supported in part by the Swiss National Science Foundation.

References

[1] A. Marinoni, S. Coda, R. Chavan, and G. Pochon, Review of Scientific Instruments **77**, 10E929 (2006).

[2] S. Coda and M. Porkolab, Review of Scientific Instruments **66**, 454 (1995).

[3] F. Jenko, W. Dorland, M. Kotschenreuther, and B. N. Rogers, Physics of Plasmas **7**, 1904 (2000).

[4] G. Merlo, Ph.D. Thesis, EPFL (2016).

[5] F. Carpanese, Ph.D. Thesis, EPFL (2021).

[6] A. Mariani *et al.*, Physics of Plasmas **25**, 012313 (2018).

[7] C. A. de Meijere *et al.*, Plasma Physics and Controlled Fusion **56**, 072001 (2014).